Analysis of exchange terms in a projected ERPA Theory applied to the quasi-elastic (e, e') reaction.

E. Bauer *

Departamento de Física, Facultad de Ciencias Exactas, Universidad Nacional de La Plata, La Plata, 1900, Argentina.

A. Polls and A. Ramos

Departament d'Estructura i Constituents de la Matèria,

Universitat de Barcelona, Diagonal 647, E-08028, Spain.

(July 20, 2018)

Abstract

A systematic study of the influence of exchange terms in the longitudinal and transverse nuclear response to quasi-elastic (e,e') reactions is presented. The study is performed within the framework of the extended random phase approximation (ERPA), which in conjuction with a projection method permits a separation of various contributions tied to different physical processes. The calculations are performed in nuclear matter up to second order in the residual interaction for which we take a $(\pi + \rho)$ -model with the addition of the Landau-Migdal g'-parameter. Exchange terms are found to be important only for the RPA-type contributions around the quasielastic peak.

Typeset using REVT_EX

^{*}Fellow of the Consejo Nacional de Investigaciones Científicas y Técnicas, CONICET.

I. INTRODUCTION

The nuclear response to an electromagnetic probe is a common tool to investigate the behaviour of the atomic nucleus [1]. At variance with a hadronic probe it allows a perturbative treatment in the external operator coupling constant. In this work we will concentrate on the study of the nuclear response function for longitudinal and transverse inclusive quasi-elastic electron scattering reactions. These responses are experimentally separated [2–7], showing that a simple model like the Fermi gas fails to reproduce the experimental data. The attempts to go beyond this model can be classified in two groups. On one side there are the methods that assume the nucleus as an assembly of non interacting nucleons with individual properties, such as the charge radius, modified with respect to the vacuum due to the presence of the other nucleons [8–11]. Another option is to explore the possibilities of a rigorous many-body theory [12–36] keeping the nucleons as the essential degrees of freedom with the same properties as in the vacuum, before resorting to such exotic effects. This work falls in this second strategy.

Several approaches to the nuclear many body problem of the nucleus for these processes have been extensively analyzed in the literature [1]. Microscopic many-body theories must deal with short range correlations (SRC) originated from the short range repulsion of the nucleon nucleon (NN) interaction. Variational calculations account for SRC by introducing a Jastrow correlation factor explicitly in the wave function. In this way, it is possible to define a correlated basis function (CBF) and build a fast converging perturbation theory using this basis. There are recent studies of both the longitudinal and the transversal response for nuclear matter in this framework [16]. Alternatively, the effect of SRC can be incorporated by introducing a well behaved effective interaction of G-matrix type or the standard Landau-Migdal parameterization, with which one can perform perturbation theory to build other correlations, for instance of RPA type. As it is not our aim to describe the full set of approaches, we will comment only on the ones which lead to our particular theory, which is based on the perturbative approach.

A simple way to introduce in the response the nucleon-nucleon correlations originated by the residual interaction is by means of the RPA theory, where one particle-one hole excitations are summed up to infinite order. Although improving the Fermi gas picture, the RPA approximation is not able to explain some features of the response as, for instance, the strength in the "dip" region of the transverse response.

An improvement upon the RPA-theory consists of allowing the coupling of one particle-one hole states to two particle-two hole ones. This corresponds to what has been called final state correlations. Two formalisms study this kind of processes. One is the second RPA (SRPA) theory (see Ref. [15] and references therein) and the other is the Green function scheme of Ref. [17] (see also [18–21]). The first one introduces final state correlations over the particle-hole bubbles of the RPA theory. In the second one the relationship between forward virtual Compton scattering and inclusive electron scattering is used to construct a one-body approximation to quasi-elastic electron scattering. In fact, at large momentum transfers, where the effect of long range correlations is negligible, the SRPA and the optical model Green's function approach should coincide [18].

Both the SRPA and the optical-model Green function approaches use the full residual interaction and allow for many particle-many hole final states. Still in both approaches the

one body external operator is limited to create (or destroy) a one particle-one hole pair. Once the external operator is allowed to scatter a particle (or hole), then two particle-two hole states stemming from ground state correlations (GSC) could be activated. The importance of these GSC are particularly relevant in the dip region for the transverse channel [23]. A theory to calculate the response function which takes into account all the above requirements is already established as the Extended RPA (ERPA) theory [25,27]. Still, the application of the ERPA theory is in general a prohibitively large task. In Ref. [30] we developed a projection method which extracts the main ingredients of the ERPA theory. In that work, the scheme was presented and the response was calculated neglecting the exchange part in the matrix elements of the nuclear particle-hole interaction. Therefore it seems necessary to complete the scheme by investigating and stablishing the influence of the exchange graphs in the longitudinal and transverse response of non-relativistic nuclear matter. Actually, the importance of the exchange terms in the RPA theory is a well known problem which can not be satisfactorily solved for finite range interactions, although several attempts have been made. In a previous work [31], we developed a simple scheme to evaluate the full antisymmetric RPA series contributing to the nuclear matter response, with the result that exchange contributions are important, specially at low momentum transfer, and can not be accounted for by simply evaluating the ring (direct) series with an effective g' parameter.

In view of the importance of the RPA exchange terms and the ongoing efforts to improve the description of the nuclear response it seems appropriate to explore whether the exchange terms in the remaining types of diagrams contained in the ERPA scheme are also important. In this work, we undertake this task and evaluate for the first time the contribution of the exchange terms to the nuclear response up to second order in the effective interaction.

The paper is organized as follows. In Sect. 2 we present the formalism. In Sect. 3 the results for the exchange contributions to the nuclear matter structure function are presented and compared with the corresponding direct ones. Finally, the conclusions are summarized in Sect. 4.

II. FORMALISM

The Longitudinal (L) and Transverse (T) structure functions, $S_{L,T}(\mathbf{q},\hbar\omega)$, are defined as

$$S_{L,T}(\boldsymbol{q},\hbar\omega) = -\frac{1}{\pi} Im < 0|\mathcal{O}_{L,T}^{\dagger}G(\hbar\omega)\mathcal{O}_{L,T}|0>, \qquad (1)$$

where $\hbar\omega$ represents the excitation energy and q the magnitude of the three momentum transfer. The nuclear ground state is denoted by $|0\rangle$ while the polarization propagator $G(\hbar\omega)$ is given by

$$G(\hbar\omega) = \frac{1}{\hbar\omega - H + i\eta} - \frac{1}{\hbar\omega + H - i\eta} , \qquad (2)$$

where H is the nuclear Hamiltonian. Explicit forms for the external excitation operators $\mathcal{O}_{L,T}$ are given by

$$\mathcal{O}_L = \sum_{j=1}^A \frac{1 + \tau_3(j)}{2} e^{i\boldsymbol{q} \cdot \boldsymbol{x}_j}, \tag{3}$$

$$\mathcal{O}_{T} = \frac{1}{2mq} \sum_{i=1}^{A} \left\{ \frac{1 + \tau_{3}(j)}{2} [\boldsymbol{q} \times \{\boldsymbol{p}_{j}, e^{i\boldsymbol{q} \cdot \boldsymbol{x}_{j}}\}] + i \frac{\mu_{s} + \mu_{v} \tau_{3}(j)}{2} [\boldsymbol{q} \times (\boldsymbol{\sigma}(j) \times \boldsymbol{q})] e^{i\boldsymbol{q} \cdot \boldsymbol{x}_{j}} \right\}, \quad (4)$$

where m is the nucleonic mass, $\boldsymbol{x_j}$ and $\boldsymbol{p_j}$ denote the position and momentum operators for individual nucleons, and $\mu_s = 0.88$, $\mu_v = 4.70$ are related to the proton and neutron magnetic moments. In fact, \mathcal{O}_L is the charge density operator while \mathcal{O}_T is related to the convection and magnetization current density. The structure functions are related to the response functions, $R_{L,T}(\boldsymbol{q},\hbar\omega)$, through the usual dipole electromagnetic form factor $G_E(q,\hbar\omega)$:

$$G_E(q, \hbar\omega) = \left[1 + \frac{(\hbar cq)^2 - (\hbar\omega)^2}{(839 \text{MeV})^2}\right]^{-2}.$$
 (5)

We introduce now the usual projection operator P, which projects into npnh configurations with n=0, 1, defined respect to the HF vacuum, which corresponds to the case n=0 and is denoted by | >. In addition, two projection operators Q and R are introduced. The action of Q(R) is to project onto the npnh space with n being an even integer greater or equal to two (n odd greater or equal to three). Explicit expressions are given by

$$P = \sum_{n = 0, 1} |n > < n|, \tag{6}$$

$$Q = \sum_{\substack{n \text{ even} \\ n \ge 2}} |n > < n|, \tag{7}$$

$$R = \sum_{\substack{n \text{ odd} \\ n > 3}} |n > < n| , \qquad (8)$$

where $|n\rangle$ indicates a *npnh* configuration.

In the literature only one projection operator, which is the sum of Q and R, is usually used. The present separation is done for convenience as it helps to clarify the role of 3p3h configurations (see Ref. [30]). It is easy to verify that P + Q + R = 1, $P^2 = P$, $Q^2 = Q$, $R^2 = R$ and PQ = QP = PR = RP = QR = RQ = 0.

Inserting the identity in Eq. (1) one obtains

$$S = S_{PP} + S_{PQ} + S_{QP} + S_{QQ} + S_{PR} + S_{RP} + S_{RR} + S_{QR} + S_{RQ} , \qquad (9)$$

where, for simplicity, we have omitted the subscripts L, T. The expression for S_{PP} is given by

$$S_{PP}(\boldsymbol{q}, \hbar\omega) = -\frac{Im}{\pi} < 0|\mathcal{O}^{\dagger}PG(\hbar\omega)P\mathcal{O}|0>;$$
(10)

and similar expressions can be written for S_{PQ} , etc. To evaluate the propagators PGP, PGQ, etc., one has to solve the following equation:

$$\mathcal{G} \cdot \mathcal{G}^{-1} = I,\tag{11}$$

where

$$\mathcal{G} = \begin{pmatrix} PGP & PGQ & PGR \\ QGP & QGQ & QGR \\ RGP & RGQ & RGR \end{pmatrix}, \qquad I = \begin{pmatrix} P & 0 & 0 \\ 0 & Q & 0 \\ 0 & 0 & R \end{pmatrix}.$$

This is an easy task once the properties of the projection operators are employed. Keeping terms up to second order in the nuclear interaction, all 3p3h final state contributions cancel each other [30]. Thus, from all terms of Eq. (9), only S_{PP} , S_{QP} (S_{PQ}) and S_{QQ} survive:

$$S_{PP} = -\frac{Im}{\pi} < 0|\mathcal{O}^{\dagger}P \frac{1}{\hbar\omega - H - \Sigma^{PQP} - Re\Sigma^{PRP} + i\eta} P\mathcal{O}|0\rangle, \tag{12}$$

$$S_{QP} = -\frac{Im}{\pi} < 0|\mathcal{O}^{\dagger}P\frac{1}{\hbar\omega - H_0 + i\eta} PH_{res}Q\frac{1}{\hbar\omega - H_0 + i\eta} Q\mathcal{O}|0\rangle, \tag{13}$$

and

$$S_{QQ} = -\frac{Im}{\pi} < 0|\mathcal{O}^{\dagger}Q\frac{1}{\hbar\omega - H_0 + i\eta} Q\mathcal{O}|0>, \tag{14}$$

where S_{QP} equals S_{PQ} . The self energy operators introduced in Eq. (12) are given by

$$\Sigma^{PQP} = PH_{res}Q\frac{1}{\hbar\omega - H_0 + i\eta} QH_{res}P$$
 (15)

and

$$Re\Sigma^{PRP} = -PH_{res}R\frac{\mathcal{P}}{\hbar\omega - H_0}RH_{res}P,$$
(16)

where \mathcal{P} denotes the principal value. We have separated the total Hamiltonian H into a one-body part, H_0 , and a residual interaction, H_{res} .

As pointed out in Ref. [30], there is still a contribution stemming from a 3p3h configuration given by the real part of 3p3h-self-energy insertion ($Re\Sigma^{PRP}$) in Eq. (12). That is, up to second order, no 3p3h physical state is possible, but virtual intermediate 3p3h configurations produce a shift in the ground state energy (see Ref. [30] and Ref. [26] for more details). The next step is to establish the structure of the ground state. Including the ground state correlations perturbatively one gets, up to first order in the residual interaction,

$$|0> = | > -H_0^{-1}QH_{res}P| > ,$$
 (17)

with | > being the Hartree Fock ground state. More explicitly, one can write

$$|0> = | > -\sum_{2} \frac{\langle 2|H_{res}| >}{\varepsilon_{gsc}} |2>,$$
 (18)

where the quantity ε_{gsc} refers to the energy of the first order correction to the ground state energy.

The aim of this section is to present the formalism showing explicitly antisymmetric matrix elements. The guidelines to obtain analytical expressions are given in Ref. [30], where direct contributions were studied. To complete the scheme, expressions for the exchange self-energy insertions are given in Appendix A and exchange terms to the structure function are presented in Appendix B. Also, and in order to simplify the calculation, we will limit ourselves to the case in which the external operator is attached to the same bubble. We will study some exceptions to this as a consequence of antisymmetrization. The three non vanishing contributions, S_{PP} , S_{QP} and S_{QQ} , will be analyzed separately below. Special attention will be paid to S_{PP} as its structure is very rich and represents the main contribution to the response function.

A. S_{PP} contribution:

Let us carefully analyze all graphs stemming from S_{PP} . To do this, we first insert the definition of P given by Eq. (6) into S_{PP} [Eq. (12)]:

$$S_{PP} = -\frac{1}{\pi} Im \sum_{n,n'=1} \langle 0|\mathcal{O}^{\dagger}|n\rangle \langle n|\frac{1}{\hbar\omega - H_0 - H_{res} - \Sigma^{PQP} - Re\Sigma^{PRP} + i\eta}$$

$$|n'\rangle \langle n'|\mathcal{O}|0\rangle. \tag{19}$$

Using the ground state given by Eq. (18) in the expression and neglecting all third and higher orders terms except the ones with self energy insertions, one can write

$$S_{PP} = S_{PP}^{Lindhard+self-energy} + S_{PP}^{first \, order \, RPA} + S_{PP}^{second \, order \, RPA}, \tag{20}$$

where

$$S_{PP}^{Lindhard+self-energy} = -\frac{1}{\pi} Im \sum_{1,1'} < |\mathcal{O}^{\dagger}|1 > < 1| \frac{1}{\hbar\omega - H_0 - \Sigma^{PQP} - Re\Sigma^{PRP} + i\eta}$$

$$|1' >_a < 1'|\mathcal{O}| > , \quad (21)$$

$$S_{PP}^{first\,order\,RPA} = -\frac{1}{\pi} Im \{ \sum_{1,1'} < |\mathcal{O}^{\dagger}| 1 > \frac{1}{\hbar\omega - \varepsilon_1 + i\eta} < 1 | H_{res}| 1' >_a$$

$$\frac{1}{\hbar\omega - \varepsilon_{1'} + i\eta} < 1' |\mathcal{O}| >$$

$$-2 \sum_{1} \sum_{2} \frac{< |H_{res}| 2 >_a}{\varepsilon_{gsc}} < 2 |\mathcal{O}^{\dagger}| 1 > \frac{1}{\hbar\omega - \varepsilon_1 + i\eta} < 1 |\mathcal{O}| > \} , \quad (22)$$

$$S_{PP}{}^{second\:order\:RPA} = -\frac{1}{\pi}\:Im\{\sum_{1,1',1''} < |\mathcal{O}^{\dagger}|1 > \frac{1}{\hbar\omega - \varepsilon_1 + i\eta} \: < 1|H_{res}|1' >_a$$

$$\frac{1}{\hbar\omega - \varepsilon_{1'} + i\eta} < 1'|H_{res}|1''>_{a}$$

$$\frac{1}{\hbar\omega - \varepsilon_{1''} + i\eta} < 1''|\mathcal{O}| >$$

$$-2\sum_{1,1''} \sum_{2} \frac{\langle |H_{res}|2>_{a}}{\varepsilon_{gsc}} < 2|\mathcal{O}^{\dagger}|1>$$

$$\frac{1}{\hbar\omega - \varepsilon_{1} + i\eta} < 1|H_{res}|1'>_{a} \frac{1}{\hbar\omega - \varepsilon_{1'} + i\eta} < 1'|\mathcal{O}| >$$

$$+\sum_{1} \sum_{2,2'} \frac{\langle |H_{res}|2>_{a}}{\varepsilon_{gsc}} < 2|\mathcal{O}^{\dagger}|1>$$

$$\frac{1}{\hbar\omega - \varepsilon_{1} + i\eta} < 1|\mathcal{O}|2'> \frac{\langle 2|H_{res}|>_{a}}{\varepsilon_{gsc}} \}, \qquad (23)$$

and $H_0|n>=\varepsilon_n|n>$.

From Eqs. (15) and (16) the self-energy insertions read now

$$<1|\Sigma^{PQP}|1'> = \sum_{2} <1|H_{res}|2>_{a} \frac{1}{\hbar\omega - \varepsilon_{2} + i\eta} <2|H_{res}|1'>_{a},$$
 (24)

and

$$<1|Re\Sigma^{PRP}|1'> = -\sum_{a}<1|H_{res}|3>_{a}\frac{\mathcal{P}}{\hbar\omega-\varepsilon_{3}}<3|H_{res}|1'>_{a}.$$
 (25)

In all expressions we have made explicit indication of antisymmetric matrix elements.

In Fig. 1 some graphs contributing to S_{PP} are shown. Within brackets we have collected direct plus exchange contributions. Let us start by analyzing the contribution to $S_{PP}^{Lindhard+self-energy}$. The presence of self energy operators makes the energy denominators in the r.h.s. of Eq. (21) to be non diagonal in our particle-hole basis. Non diagonal terms, shown by graphs SE2D, SE2E and SE2E' in Fig. 1, are evaluated at second order. For diagonal ones, shown by graphs SE1D, SE1E, SE3D and SE3E in Fig. 1, we first build up an antisymmetric self-energy insertion and then sum it up to infinite order.

The first two orders leading to the RPA response (eqs. (22) and (23)), are shown by graphs RPA1D to RPA2E' in Fig. 1, where only the forward going contributions are explicitly shown, that is, the ones stemming from the first terms on the r.h.s. of the above mentioned equations. If exchange terms were neglected one would be able to sum terms up to infinite order leading to the usual ring series.

As mentioned, in this paper we keep terms up to second order in the evaluation of exchange contributions. However, for the RPA type diagrams we use the method described in Ref. [31], which allows to effectively sum up the full antisymmetric RPA series. That method is based on splitting the interaction into a pure contact part and a remaining part

chosen such that the second-order ring coincides with the full ring series. The pure contact term allows a straightforward evaluation of the antisymmetric RPA series up to infinite order, while only terms up to second order are retained for the remaining part of the interaction.

B. S_{QP} contribution:

Using the definition of P and Q into S_{QP} [Eq. (13)] we have

$$S_{QP} = -2\frac{1}{\pi} Im \{ \sum_{1,2,2'} < |\mathcal{O}^{\dagger}| 1 > \frac{1}{\hbar\omega - \varepsilon_1 + i\eta} < 1 | H_{res}| 2 >_a$$

$$\frac{1}{\hbar\omega - \varepsilon_2 + i\eta} < 2 |\mathcal{O}| 2' > \frac{<2' | H_{res}| >_a}{\varepsilon_{asc}} \}.$$
(26)

Note that as \mathcal{O} is a one body operator, it can scatter a particle (or hole) or create (or destroy) a particle-hole pair. That is, the Hartree-Fock ground state is not connected to a 2p2h configuration through \mathcal{O} .

In Fig. 2 we present the second order contributions to S_{QP} . As a consequence of antisymmetrization, a direct term where the external operator is attached to a different bubble has come into play (given by graph SQPD' of this figure). Naturally, when we act with the antisymmetrization operator over this term, the same set of graphs appears. We account for this through a factor two.

C. S_{QQ} contribution:

Finally, the expression for S_{QQ} [Eq. (14)] is simply

$$S_{QQ} = -\frac{1}{\pi} Im \left\{ \sum_{2,2',2''} \frac{\langle |H_{res}|2\rangle_a}{\varepsilon_{gsc}} \langle 2|\mathcal{O}^{\dagger}|2'\rangle \frac{1}{\hbar\omega - \varepsilon_{2'} + i\eta} \langle 2'|\mathcal{O}|2''\rangle \right.$$

$$\frac{\langle 2''|H_{res}|\rangle_a}{\varepsilon_{gsc}} \right\}. \tag{27}$$

Here, the only possible action for the external operator is to scatter a particle or a hole.

In Fig. 3, we present the main contributions to S_{QQ} . Graphs SQQ3D' presents a direct contribution with the external operator attached to a different bubble, in complete analogy with S_{QP} .

III. RESULTS FOR NUCLEAR MATTER

In order to benefit from the advantage of translational invariance, results have been obtained for infinite nuclear matter at normal saturation density corresponding to a Fermi momentum $k_F = 1.36 \text{ fm}^{-1}$.

For the residual interaction H_{res} we assume the ($\pi + \rho$)-exchange model at the static limit with the addition of the Landau Migdal g'-parameter. In pionic units it reads

$$H_{res}(l) = \frac{f_{\pi}^{2}}{\mu_{\pi}^{2}} \Gamma_{\pi}^{2}(l) (\tilde{g}'(l)\boldsymbol{\tau} \cdot \boldsymbol{\tau'} \boldsymbol{\sigma} \cdot \boldsymbol{\sigma'} + \tilde{h}'(l)\boldsymbol{\tau} \cdot \boldsymbol{\tau'} \boldsymbol{\sigma} \cdot \hat{\boldsymbol{l}} \boldsymbol{\sigma'} \cdot \hat{\boldsymbol{l}}) , \qquad (28)$$

with

$$\tilde{g}'(l) = g' - \frac{\Gamma_{\rho}^{2}(l)}{\Gamma_{\pi}^{2}(l)} C_{\rho} \frac{l^{2}}{l^{2} + \mu_{\rho}^{2}}, \qquad (29)$$

$$\tilde{h}'(l) = -\frac{l^2}{l^2 + \mu_{\pi}^2} + \frac{\Gamma_{\rho}^2(l)}{\Gamma_{\pi}^2(l)} C_{\rho} \frac{l^2}{l^2 + \mu_{\rho}^2} , \qquad (30)$$

where $\mu_{\pi}\hbar c$ ($\mu_{\rho}\hbar c$) is the pion (rho) rest mass and $C_{\rho} = 2.18$. For the form factor of the πNN (ρNN) vertex we have taken

$$\Gamma_{\pi,\rho}(l) = \frac{\Lambda_{\pi,\rho}^2 - (\mu_{\pi,\rho}\hbar c)^2}{\Lambda_{\pi,\rho}^2 + (\hbar c l)^2} , \qquad (31)$$

with $\Lambda_{\pi} = 1.3$ GeV and $\Lambda_{\rho} = 2$. GeV. The role of the g'-parameter is to account for short range correlations. Note that for a pure contact interaction exchange contributions have been traditionally included in the RPA series by a redefinition of the Landau-Migdal parameters. In particular, standard g'-values range from 0.7 to 0.95 but, when redefined to account for antisymmetric terms, the values are lowered and range from 0.5 to 0.7 [37]. As we evaluate explicitly exchange graphs a standard g'-value from 0.7 to 0.95 should be used. We have employed the value g' = 0.7. In addition, in all the diagrams considered in our calculations, the nucleon lines have been dressed in an average way by taking a momentum independent effective mass value of $m^*/m = 0.85$.

From Eqs. (21)-(27), explicit expressions for the structure functions in nuclear matter can be obtained, where the sums over the different configurations are replaced by multidimensional integrals. The expressions of the direct terms were reported in Ref. [30] and will not be repeated here. In Appendix A we give the exchange self-energy insertions appearing in Eq. (21) (see Eqs. (24) and (25)), while in Appendix B the exchange contributions to Eqs. (21)-(23) and (26)-(27) are shown (see also Figs. 1-3). The multiple integrations have been performed using a Monte Carlo technique.

Let us analyse the three non-vanishing contributions, S_{PP} , S_{QP} and S_{QQ} , to the response. We follow the notation already shown in Figs. 1-3.

Tables I and II give the results for the S_{PP} channel. In Table I we compare all direct and exchange contributions from self-energy insertions. To avoid divergencies, diagonal self-energy insertions are evaluated up to infinite order [24]. To do this, an average over the hole momentum of the bubble where the self-energy is attached should be done. This procedure is outlined in Appendix A. From the table it is clear that, although small in general, the exchange diagrams can amount to a non-negligible fraction of the direct ones, especially at energies around and below the quasiparticle peak. This is also visualized in Fig. 4, where the structure function including only the direct self-energy diagrams (long-dashed

line) is compared to that containing, in addition, the exchange ones (full line) for both the longitudinal (upper part) and the transverse (lower part) channels. The short-dashed line is the free structure function calculated with an effective mass of value of $m^*/m = 0.85$. As has been observed before [16,32–34], the dressing of the nucleon lines by self-energy insertions smears out the structure function, moving strength out from the quasiparticle peak to the high missing energy region.

Notice that in the diagrams shown in Figs. 1-3 we have not explicitly included the first order self-energy insertion on the fermion propagators. Instead of this, we have preferred to use a Lindhard function calculated with an effective mass m^* in the nucleon propagators and, therefore, it already contains in an average way the effects of those self-energy insertions propagated to all orders. Actually, the use of m^* is equivalent to having a real and energy independent self-energy parameterized by a function quadratic in the momentum of the nucleon. These mean field single-particle states define the HF ground state and the basis in which the perturbation theory has been constructed.

The second order self-energy diagrams SE1D,SE3D,SE1E,SE3E are responsible for the appearance of an imaginary part which yields a width to the nucleon lines, which in turn is the responsible for the observed spreading in the nuclear response.

In Table II we analyse the RPA-type correlations showing explicit results for the first and second order contributions. This is done for the transverse channel as RPA-type correlations are zero for the longitudinal one due to the election of our interaction with no f or f' Landau-Migdal terms. In the last column we also present the results for RPA correlations when exchange contributions are included up to infinite order, following the scheme of Ref. [31]. From Table II is clear that exchange terms of RPA type are very important. Their size is comparable (even bigger) to other direct diagrammatic contributions to the structure function and, therefore, they should not be neglected. Given the magnitude of these RPA exchange terms, the differences between the next-to-last and last columns of Table II also suggest that it is important to sum them up to infinite order as was done in Ref. [31]. The effect of the RPA diagrams in the transverse structure function is also displayed in Fig. 5, where the full antisymmetric RPA series (full line) is compared to the direct ring series (long-dashed line). We observe that the transfer of strength from the low to the high energy region typical of the polarization (ring) diagrams is partly restored by the incorporation of the exchange diagrams.

In Table III, we study the S_{QP} channel. In this kind of graphs the external operator creates (or destroys) a particle-hole pair and scatters a particle (or a hole). We have evaluated the case where the external operator scatters a particle. The case where it scatters a hole is negligible as can be found in Ref. [30]. As mentioned above, due to the action of the antisymmetrization operator a graph where the external operator is attached to different bubbles has to be considered. This graph is SQPD' in Fig. 2 and has some influence as can be seen from Table III. The other exchange graphs are negligible.

In Table IV the results for the S_{QQ} channel are shown. As for the S_{QP} channel, exchange graphs are very small. The importance of the ground state correlation diagrams is clearly seen in Fig. 6, where the full lines represent the addition of $S_{QP} + S_{QQ}$ to the long-dashed lines, which contain the S_{PP} contributions. In the longitudinal channel (upper part), only the self-energy terms contribute to S_{PP} , while the transverse channel (lower part) contains, in addition, the RPA-type correlations. In view of these results it is clear that incorporating

the S_{QP} and S_{QQ} channels is necessary in any perturbative calculation of the nuclear matter response as observed in Ref. [30]. Having established in this work the smallness of the corresponding exchange terms is particularly interesting, since the calculation of these channels can be restricted to the direct graphs thus avoiding a great deal of numerical computations.

In addition our findings also support the idea that the use of an effective g' to account for exchange terms in the nuclear response is not appropriate. This point was already raised in Ref. [31], where we built a prescription to calculate the full antisymmetric RPA series of the nuclear response. In that work, we showed that the use of a standard average prescription for g' was not able to reproduce the RPA antisymmetric response, especially for intermediate values of the momentum transfer. Using the average g' for calculating the other types of correlations would not be appropriate either because we have shown that they are basically dominated by the direct contributions. This is visualized in Table V where, changing the g' parameter to an effective value of g' = 0.5 does not, in the first place, reproduce the antisymmetric RPA response contained implicitly in the first column of the transverse part (a point already raised in Ref. [31]) but also induces non negligible modifications in the other contributions, especially those related to ground state correlations (compare the next-to-last and last columns).

From our study we conclude that the nuclear response is basically dominated by the direct diagrams and the exchange ones only need to be considered (and to all orders) for the RPA type correlations.

IV. CONCLUSIONS

A projection method to extract the main contributions of the ERPA theory with the explicit inclusion of exchange terms has been developed. This work is a continuation of a previous one [30] in which only direct terms were studied. Here we have tried to clarify the importance of exchange terms of the particle-hole interaction, by performing a quantitative analysis of their influence in the nuclear response.

The projection method classifies the contributions to the nuclear structure function into three channels, called S_{PP} , S_{QP} and S_{QQ} with P and Q being projections operators defined in Sect. 1. This separation permits to study the effects of the different types of correlations. In this sense, S_{PP} represents final state correlations, S_{QQ} ground state correlations and S_{QP} the interference between them. Through the analysis of our results we can conclude that all types of correlations are important and should be considered when one studies the nuclear response.

After this statement, the the problem is the big number of graphs which should be evaluated when the exchange part of the nucleon-nucleon interaction is retained. Before the numerical calculation we can see no reason to neglect any contribution. Our calculations show that for final state correlations, i.e. self-energy insertions and mainly RPA-type correlations, the exchange graphs are relevant in agreement with Refs. [37,38]. On the other hand, they can be neglected for ground state correlations. Also, within the energy-momentum region under consideration, exchange terms can not be parameterized by a redefinition of the g' parameter.

It is also important to stress that the interaction employed and in particular the value for g', comes from parameterizations of processes at a lower energy-momentum region than

the ones considered here. Those values do not necessarily hold for us. Also from Table V, we see that a small change in one parameter can produce a noticeable change in the structure function. In any case, our scope was not a search of the optimal paremeters that produce a good agreement with the experimental data but a careful analysis of the exchange diagrams and our conclusions should remain valid in a wide variety of situations.

In summary, our study shows that the nuclear response is basically dominated by the direct diagrams, the most relevant being those of Figs. 1-3, and the exchange contributions only need to be considered (and to all orders) for the RPA type correlations, which can be evaluated using the prescription of Ref. [31].

APPENDIX A

In this appendix we show explicit expressions for exchange contributions to the self-energy insertions Direct contributions can be found in Ref. [30]. Exchange self-energy insertions from eqs. (24) and (25) (which contribute to graphs SE1E and SE3E of Fig. 1, respectively), are given by

$$(\Sigma^{PQP}(\boldsymbol{Q}, \nu, \boldsymbol{h}))^{part.\,exch.} = -\frac{1}{(2\pi)^4} \left(\frac{f_{\pi}^2}{4\pi\hbar c}\right)^2 \frac{mc^2 k_F^4}{\mu_{\pi}^4} \int d^3k \int d^3k' \; \theta(|\boldsymbol{h} + \boldsymbol{Q} - \boldsymbol{k}| - 1)$$

$$\theta(1 - |\boldsymbol{h} + \boldsymbol{Q} - \boldsymbol{k} - \boldsymbol{k'}|) \theta(|\boldsymbol{h} + \boldsymbol{Q} - \boldsymbol{k'}| - 1) \Gamma_{\pi}^2(k) \Gamma_{\pi}^2(k')$$

$$(3\tilde{g}'^2 - (2(\hat{\boldsymbol{k}}.\hat{\boldsymbol{k'}})^2 - 1)\tilde{h}'^2 + 2\tilde{g}'\tilde{h}')$$

$$\frac{1}{\nu - (Q^2/2 + \boldsymbol{h}.\boldsymbol{Q} - \boldsymbol{k}.\boldsymbol{k'}) + i\eta}$$
(32)

and

$$(Re \Sigma^{PRP}(\boldsymbol{Q}, \nu, \boldsymbol{h}))^{part. \, exch.} = \frac{1}{(2\pi)^4} \left(\frac{f_{\pi}^2}{4\pi\hbar c} \right)^2 \frac{mc^2 \, k_F^4}{\mu_{\pi}^4} \int d^3k \, \int d^3k' \, \theta(1 - |\boldsymbol{h} + \boldsymbol{Q} - \boldsymbol{k}|)$$

$$\theta(|\boldsymbol{h} + \boldsymbol{Q} - \boldsymbol{k} - \boldsymbol{k'}| - 1)\theta(1 - |\boldsymbol{h} + \boldsymbol{Q} - \boldsymbol{k'}|)\Gamma_{\pi}^2(k)\Gamma_{\pi}^2(k')$$

$$(3\tilde{g}'^2 - (2(\hat{\boldsymbol{k}}.\hat{\boldsymbol{k'}})^2 - 1)\tilde{h}'^2 + 2\tilde{g}'\tilde{h}')$$

$$\frac{1}{\nu - (Q^2/2 + \boldsymbol{h}.\boldsymbol{Q} + \boldsymbol{k}.\boldsymbol{k'})}.$$
(33)

We have used dimensionless quantities $\mathbf{Q} = \mathbf{q}/k_F$ and $\nu = \hbar\omega/2\varepsilon_F$; k_F and ε_F being the Fermi momentum and energy, respectively.

In order to simplify the calculation, it is a good approximation to eliminate the dependence on the hole momentum, by an average procedure (see Ref. [30]), as follows

$$\Sigma^{PQ(R)P}(\boldsymbol{Q},\nu) \equiv \frac{1}{\frac{4}{3}\pi} \int d^3h \ \Sigma^{PQ(R)P}(\boldsymbol{Q},\nu,\boldsymbol{h})$$
 (34)

APPENDIX B

In this appendix we show explicit expressions for exchange contributions to the structure function. Direct contributions can be found in Ref. [30].

Let us first consider the S_{PP} channel. Graph SE2E of Fig. 1 (see Eq. (21)) is given by,

$$(S_{SE1}(\mathbf{Q}, \nu))_{L,T} = -\frac{A}{(2\pi)^5} \left(\frac{f_{\pi}^2}{4\pi\hbar c}\right)^2 \frac{3(mc^2)^3}{2(\hbar c\mu_{\pi})^4} \int d^3h \int d^3k \int d^3k' \, \mathcal{OV}_{(L,T),SE2E}$$

$$\theta(1 - |\mathbf{h}|)\theta(|\mathbf{h} + \mathbf{Q}| - 1)\theta(1 - |\mathbf{h} + \mathbf{k'}|)\theta(|\mathbf{h} + \mathbf{k} + \mathbf{k'}| - 1)$$

$$\theta(1 - |\mathbf{h} + \mathbf{k}|)\theta(|\mathbf{h} + \mathbf{k} + \mathbf{Q}| - 1)(\frac{-1}{\pi} Im)\left[\frac{1}{\nu - (Q^2/2 + \mathbf{Q}.\mathbf{h}) + i\eta}\right]$$

$$\frac{1}{\nu - (Q^2/2 + \mathbf{Q}.\mathbf{h} + \mathbf{k}.\mathbf{k'}) + i\eta} \frac{1}{\nu - (Q^2/2 + \mathbf{Q}.(\mathbf{h} + \mathbf{k})) + i\eta}\right]. \quad (35)$$

Graph SE2E' of Fig. 1 (see Eq. (21)):

$$(S_{SE2E'}(\boldsymbol{Q}, \nu))_{L,T} = -\frac{A}{(2\pi)^5} \left(\frac{f_{\pi}^2}{4\pi\hbar c}\right)^2 \frac{3(mc^2)^3}{2(\hbar c\mu_{\pi})^4} \int d^3h \int d^3k \int d^3k' \, \mathcal{OV}_{(L,T),SE2E'}$$

$$\theta(1 - |\boldsymbol{h}|)\theta(|\boldsymbol{h} + \boldsymbol{Q}| - 1)\theta(1 - |\boldsymbol{h} + \boldsymbol{k}|)\theta(1 - |\boldsymbol{h} + \boldsymbol{k} + \boldsymbol{k'} + \boldsymbol{Q}|)$$

$$\theta(|\boldsymbol{h} + \boldsymbol{k'} + \boldsymbol{Q}|)\theta(|\boldsymbol{h} + \boldsymbol{k} + \boldsymbol{Q}| - 1)\left(\frac{-1}{\pi} Im\right)\left[\frac{1}{\nu - (Q^2/2 + \boldsymbol{Q}.\boldsymbol{h}) + i\eta}\right]$$

$$\frac{1}{\nu - (Q^2/2 + \boldsymbol{Q}.\boldsymbol{h} - \boldsymbol{k}.\boldsymbol{k'}) + i\eta} \frac{1}{\nu - (Q^2/2 + \boldsymbol{Q}.(\boldsymbol{h} + \boldsymbol{k})) + i\eta}\right], \quad (36)$$

where

and

$$\mathcal{OV}_{L,SE2E} = \mathcal{OV}_{L,SE2E'} = \Gamma_{\pi}^{2}(k) \; \Gamma_{\pi}^{2}(k') \; \{3\tilde{g}^{2} - (2(\hat{k}.\hat{k'})^{2} - 1)\tilde{h}^{2} + 2\tilde{g}'\tilde{h}'\} \; , \tag{37}$$

$$\mathcal{OV}_{T,SE2E} = \mathcal{OV}_{T,SE2E'} =$$

$$= (\frac{\hbar c k_F}{2mc^2})^2 \Gamma_{\pi}^2(k) \Gamma_{\pi}^2(k') \{4[\boldsymbol{h}.(\boldsymbol{h}+\boldsymbol{k}) - (\widehat{\boldsymbol{Q}}.\boldsymbol{h})(\widehat{\boldsymbol{Q}}.(\boldsymbol{h}+\boldsymbol{k}))]$$

$$[3\tilde{g}'^2 - (2(\widehat{\boldsymbol{k}}.\widehat{\boldsymbol{k'}})^2 - 1)\tilde{h}'^2 + 2\tilde{g}'\tilde{h}'] +$$

$$(-3\mu_s^2 + \mu_v^2)[Q^2\tilde{g}'^2 + ((\boldsymbol{Q}.\boldsymbol{k'})^2 - 2(\boldsymbol{k}.\boldsymbol{k'})(\boldsymbol{Q}.\boldsymbol{k})(\boldsymbol{Q}.\boldsymbol{k'}))\tilde{h}'^2 +$$

$$(\boldsymbol{Q}.\widehat{\boldsymbol{k'}})^2 \tilde{g}'(k)\tilde{h}'(k') + (Q^2 - 2(\boldsymbol{Q}.\widehat{\boldsymbol{k}})^2)\tilde{g}'(k')\tilde{h}'(k)] -$$

$$(-3\mu_s + \mu_v)\tilde{h}'^2 \frac{2}{Q^2} (\widehat{\boldsymbol{k}}.\widehat{\boldsymbol{k'}})[(\widehat{\boldsymbol{k}}.\boldsymbol{Q})\widehat{\boldsymbol{k'}}.(2\boldsymbol{h}+\boldsymbol{k}) - (\widehat{\boldsymbol{k'}}.\boldsymbol{Q})\widehat{\boldsymbol{k}}.(2\boldsymbol{h}+\boldsymbol{k})]\} . \tag{38}$$

First order exchange contribution to the RPA-type correlation (see Eq. (22) and graph RPA1E of Fig. 1):

$$(S_{RPA1E}(\mathbf{Q}, \nu))_{L,T} = -\frac{A}{(2\pi)^3} \left(\frac{f_{\pi}^2}{4\pi\hbar c} \right) \frac{3(mc^2)^2}{2(\hbar c\mu_{\pi})^2 \hbar ck_F} \int d^3h \int d^3k \, \mathcal{OV}_{(L,T),RPA1E}$$

$$\theta(1-h)\theta(|\mathbf{h}+\mathbf{Q}|-1)\theta(1-|\mathbf{h}+\mathbf{k}|)\theta(|\mathbf{h}+\mathbf{k}+\mathbf{Q}|-1)$$

$$(-\frac{1}{\pi} Im) \left\{ \left(\frac{1}{2\nu - (Q^2 + 2\mathbf{h}.\mathbf{Q}) + i\eta} - \frac{1}{2\nu + (Q^2 + 2\mathbf{h}.\mathbf{Q})} \right) \right.$$

$$\left(\frac{1}{2\nu - (Q^2 + 2(\mathbf{h}+\mathbf{k}).\mathbf{Q}) + i\eta} - \frac{1}{2\nu + (Q^2 + 2(\mathbf{h}+\mathbf{k}).\mathbf{Q})} \right) \right\}, (39)$$

where

$$\mathcal{OV}_{(L),RPA1E} = \Gamma_{\pi}^{2}(k)(3\tilde{g}' + \tilde{h}') \tag{40}$$

and

$$\mathcal{OV}_{(T),RPA1E} = \left(\frac{\hbar c k_F}{2mc^2}\right)^2 \Gamma_{\pi}^2(k) \left\{ \left[3\tilde{g}' + \tilde{h}' \right] 4 \left[(\boldsymbol{h}.(\boldsymbol{h} + \boldsymbol{k}) - (\boldsymbol{Q}.\boldsymbol{h})\boldsymbol{Q}.(\boldsymbol{h} + \boldsymbol{k}) \right] / Q^2 \right] + \left(-3\mu_s^2 + \mu_v^2 \right) Q^2 (\tilde{g}' + \tilde{h}'(\hat{\boldsymbol{k}}.\widehat{\boldsymbol{Q}})^2 \right\}. \tag{41}$$

Graph RPA2E of Fig. 1 (see Eq. (23)):

$$(S_{RPA2E}(\mathbf{Q}, \nu))_{T} = -\frac{A}{(2\pi)^{5}} \left(\frac{f_{\pi}^{2}}{4\pi\hbar c}\right)^{2} \frac{3(mc^{2})^{3}}{(\hbar c\mu_{\pi})^{4}} \left(-\frac{1}{\pi} Im\right) \{\mathcal{L}(\mathbf{Q}, \nu)$$

$$\int d^{3}h \int d^{3}k \, \mathcal{OV}_{(L,T),RPA2E}\theta(1-h)\theta(|\mathbf{h}+\mathbf{Q}|-1)\theta(1-|\mathbf{h}+\mathbf{k}|)$$

$$\theta(|\mathbf{h}+\mathbf{k}+\mathbf{Q}|-1)\left(\frac{1}{2\nu-(Q^{2}+2\mathbf{h}\cdot\mathbf{Q})+i\eta} - \frac{1}{2\nu+(Q^{2}+2\mathbf{h}\cdot\mathbf{Q})}\right)$$

$$\left(\frac{1}{2\nu-(Q^{2}+2(\mathbf{h}+\mathbf{k})\cdot\mathbf{Q})+i\eta} - \frac{1}{2\nu+(Q^{2}+2(\mathbf{h}+\mathbf{k})\cdot\mathbf{Q})}\right) \}, \quad (42)$$

with

$$\mathcal{L}(\boldsymbol{Q}, \nu) = \int d^3 p \; \theta(|\boldsymbol{p} + \boldsymbol{Q}/2| - 1) \; \theta(1 - |\boldsymbol{p} - \boldsymbol{Q}/2|)$$

$$\left(\frac{1}{2\nu - Q^2 - 2\boldsymbol{Q} \cdot \boldsymbol{p} + i\eta} - \frac{1}{2\nu + Q^2 + 2\boldsymbol{Q} \cdot \boldsymbol{p}}\right). \tag{43}$$

and

$$\mathcal{OV}_{(T),RPA2E} = \Gamma_{\pi}^{2}(Q)\Gamma_{\pi}^{2}(k)Q^{2}4\tilde{g}'\mu_{v}^{2}(\tilde{g}' + \tilde{h}'(\hat{\boldsymbol{k}}.\widehat{\boldsymbol{Q}})^{2}). \tag{44}$$

(Note that for the present interaction the longitudinal contribution is zero). Graph RPA2E' of Fig. 1 (see Eq. (23)):

$$(S_{RPA2E'}(\mathbf{Q}, \nu))_{L,T} = \frac{A}{(2\pi)^5} \left(\frac{f_{\pi}^2}{4\pi\hbar c}\right)^2 \frac{6mc^2 k_F^2}{(\hbar c \mu_{\pi}^2)^2} \int d^3h \int d^3k \int d^3k' \, \mathcal{OV}_{(L,T),RPA2E'}$$

$$\theta(1-h)\theta(|\mathbf{h}+\mathbf{Q}|-1)\theta(1-|\mathbf{h}+\mathbf{k}|)$$

$$\theta(|\mathbf{h}+\mathbf{k}+\mathbf{Q}|-1)\theta(1-|\mathbf{h}+\mathbf{k}+\mathbf{k'}|)\theta(|\mathbf{h}+\mathbf{k}+\mathbf{k'}+\mathbf{Q}|-1)$$

$$\left(-\frac{1}{\pi} Im\right) \left\{ \left(\frac{1}{2\nu - (Q^2 + 2\mathbf{h} \cdot \mathbf{Q}) + i\eta} - \frac{1}{2\nu + (Q^2 + 2\mathbf{h} \cdot \mathbf{Q})}\right) \right.$$

$$\left(\frac{1}{2\nu - (Q^2 + 2(\mathbf{h}+\mathbf{k}) \cdot \mathbf{Q}) + i\eta} - \frac{1}{2\nu + (Q^2 + 2(\mathbf{h}+\mathbf{k}) \cdot \mathbf{Q})}\right)$$

$$\left(\frac{1}{2\nu - (Q^2 + 2(\mathbf{h}+\mathbf{k}+\mathbf{k'}) \cdot \mathbf{Q}) + i\eta} - \frac{1}{2\nu + (Q^2 + 2(\mathbf{h}+\mathbf{k}+\mathbf{k'}) \cdot \mathbf{Q})}\right) \right\},$$
(45)

where

$$\mathcal{OV}_{(L),RPA2E'} = \Gamma_{\pi}^{2}(k) \, \Gamma_{\pi}^{2}(k') 10[9(\tilde{g}')^{2} + \tilde{h}'^{2} + 6\tilde{g}'\tilde{h}']$$
(46)

and

$$\mathcal{OV}_{(T),RPA2E'} = \left(\frac{\hbar c k_F}{2mc^2}\right)^2 \Gamma_{\pi}^2(k) \Gamma_{\pi}^2(k') \left\{ 40[9(\tilde{g}')^2 + \tilde{h}'^2 + 6\tilde{g}'\tilde{h}'] \right\} \\
\left[(\boldsymbol{h}.(\boldsymbol{h} + \boldsymbol{k} + \boldsymbol{k'}) - (\boldsymbol{Q}.\boldsymbol{h})\boldsymbol{Q}.(\boldsymbol{h} + \boldsymbol{k} + \boldsymbol{k'})]/Q^2 \right] + \\
\frac{9\mu_s^2 + \mu_v^2}{2} \left\{ Q^2[(\tilde{g}'_2)^2 + \tilde{h}'^2(2(\hat{\boldsymbol{k}}.\hat{\boldsymbol{k'}})^2 - 1)] + \\
\tilde{h}'^2[(\boldsymbol{Q}.\hat{\boldsymbol{k}})^2 + (\boldsymbol{Q}.\hat{\boldsymbol{k'}})^2 - 2(\boldsymbol{Q}.\hat{\boldsymbol{k}})(\boldsymbol{Q}.\hat{\boldsymbol{k'}})(\hat{\boldsymbol{k}}.\hat{\boldsymbol{k'}})] + \tilde{g}'_2\tilde{h}'[(\boldsymbol{Q}.\hat{\boldsymbol{k}})^2 + (\boldsymbol{Q}.\hat{\boldsymbol{k'}})^2] \right\}. \tag{47}$$

Going now to the S_{QP} and S_{QQ} -channel (see Eqs. (26) and (27)); we have for graph SQPE of Fig. 2:

$$(S_{SQPE}(\boldsymbol{Q}, \nu))_{L,T} = \frac{A}{(2\pi)^5} \left(\frac{f_{\pi}^2}{4\pi\hbar c}\right)^2 \frac{3(mc^2)^3}{4(\hbar c\mu_{\pi})^4} \int d^3h \int d^3k \int d^3k' \, \mathcal{OV}_{(L,T),SQPE}$$
$$\theta(1 - |\boldsymbol{h}|)\theta(|\boldsymbol{h} - \boldsymbol{k}| - 1)\theta(|\boldsymbol{h} - \boldsymbol{k} + \boldsymbol{Q}| - 1)\theta(|\boldsymbol{h} - \boldsymbol{k'} + \boldsymbol{Q}| - 1)$$

$$\theta(|\boldsymbol{h}+\boldsymbol{Q}|-1)\theta(1-|\boldsymbol{h}-\boldsymbol{k}-\boldsymbol{k'}+\boldsymbol{Q}|)\frac{1}{\boldsymbol{k}.(\boldsymbol{k'}-\boldsymbol{Q})}$$

$$(\frac{-1}{\pi}Im)\left[\frac{1}{\nu-(Q^2/2+\boldsymbol{Q}.\boldsymbol{h}-\boldsymbol{k}.\boldsymbol{k'})+i\eta}\frac{1}{\nu-(Q^2/2+\boldsymbol{Q}.\boldsymbol{h}))+i\eta}\right].$$
(48)

Graph SQPE' of Fig. 2:

$$(S_{SQPE'}(\boldsymbol{Q}, \nu))_{L,T} = \frac{A}{(2\pi)^5} \left(\frac{f_{\pi}^2}{4\pi\hbar c}\right)^2 \frac{3(mc^2)^3}{4(\hbar c\mu_{\pi})^4} \int d^3h \int d^3k \int d^3k' \, \mathcal{OV}_{(L,T),SQPE'}$$

$$\theta(1 - |\boldsymbol{h}|)\theta(|\boldsymbol{h} - \boldsymbol{k}| - 1)\theta(|\boldsymbol{h} - \boldsymbol{k'} + \boldsymbol{Q}| - 1)\theta(|\boldsymbol{h} + \boldsymbol{Q}| - 1)$$

$$\theta(|\boldsymbol{h} - \boldsymbol{k'}| - 1)\theta(1 - |\boldsymbol{h} - \boldsymbol{k} - \boldsymbol{k'}|) \frac{1}{\boldsymbol{k}.\boldsymbol{k'}}$$

$$\left(\frac{-1}{\pi} Im\right) \left[\frac{1}{\nu - (Q^2/2 + \boldsymbol{Q}.\boldsymbol{h} - \boldsymbol{k'}.(\boldsymbol{k} + \boldsymbol{Q})) + i\eta} \frac{1}{\nu - (Q^2/2 + \boldsymbol{Q}.\boldsymbol{h})) + i\eta}\right],$$
(49)

where

$$\mathcal{OV}_{L.SOPE} = \mathcal{OV}_{L.SE2E} , \qquad (50)$$

$$\mathcal{OV}_{T,SQPE} = \mathcal{OV}_{T,SE2E} , \qquad (51)$$

$$\mathcal{OV}_{T,SQPE'} = (\frac{\hbar c k_F}{2mc^2})^2 \Gamma_{\pi}^2(k) \Gamma_{\pi}^2(k') \{4[\boldsymbol{h}.(\boldsymbol{h}+\boldsymbol{k'}) - (\widehat{\boldsymbol{Q}}.\boldsymbol{h})(\widehat{\boldsymbol{Q}}.(\boldsymbol{h}+\boldsymbol{k'})]$$

$$[3\tilde{g}'^2 - (2(\widehat{\boldsymbol{k}}.\widehat{\boldsymbol{k'}})^2 - 1)\tilde{h}'^2 + 2\tilde{g}'\tilde{h}'] +$$

$$(-3\mu_s^2 + \mu_v^2)[Q^2\tilde{g}'^2 + ((\boldsymbol{Q}.\boldsymbol{k'})^2 - 2(\boldsymbol{k}.\boldsymbol{k'})(\boldsymbol{Q}.\boldsymbol{k})(\boldsymbol{Q}.\boldsymbol{k'}))\tilde{h}'^2 +$$

$$(\boldsymbol{Q}.\widehat{\boldsymbol{k'}})^2\tilde{g}'(k)\tilde{h}'(k') + (Q^2 - 2(\boldsymbol{Q}.\widehat{\boldsymbol{k}})^2)\tilde{g}'(k')\tilde{h}'(k)] -$$

$$(-3\mu_s + \mu_v)\tilde{h}'^2 \frac{2}{Q^2} (\widehat{\boldsymbol{k}}.\widehat{\boldsymbol{k'}})[(\widehat{\boldsymbol{k}}.\boldsymbol{Q})\widehat{\boldsymbol{k'}}.(2\boldsymbol{h}+\boldsymbol{k'}) - (\widehat{\boldsymbol{k'}}.\boldsymbol{Q})\widehat{\boldsymbol{k}}.(2\boldsymbol{k}+\boldsymbol{k'})]\} .$$

$$(52)$$

Graph SQPD' of Fig. 2:

$$(S_{QPD'}(\boldsymbol{Q},\nu))_{L,T} = -\frac{A}{(2\pi)^5} \left(\frac{f_{\pi}^2}{4\pi\hbar c}\right)^2 \frac{3(mc^2)^3}{2(\hbar c\mu_{\pi})^4} \int d^3h \int d^3h' \int d^3k \,\,\mathcal{OV}_{(L,T),SQPD'}$$

$$\theta(1 - |\mathbf{h}|)\theta(|\mathbf{h} + \mathbf{Q}| - 1)\theta(|\mathbf{h} - \mathbf{k}| - 1)\theta(|\mathbf{h'} + \mathbf{k} + \mathbf{Q}| - 1)$$

$$\theta(|\mathbf{h'} + \mathbf{k}| - 1)\theta(1 - |\mathbf{h'}|)\frac{1}{k^2 - \mathbf{k} \cdot \mathbf{h} + \mathbf{k} \cdot \mathbf{h'}} \left(\frac{-1}{\pi} Im\right)$$

$$\frac{1}{\nu - (Q^2/2 + \mathbf{Q} \cdot \mathbf{h}) + i\eta} \frac{1}{\nu - (k^2 + Q^2/2 + \mathbf{k} \cdot (\mathbf{h'} - \mathbf{h}) + \mathbf{Q} \cdot (\mathbf{k} + \mathbf{h'})) + i\eta}$$
(53)

Graph SQQ3D' of Fig. 3:

$$(S_{QQ3D'}(\mathbf{Q}, \nu))_{L,T} = \frac{A}{(2\pi)^5} \left(\frac{f_{\pi}^2}{4\pi\hbar c}\right)^2 \frac{3(mc^2)^3}{2(\hbar c\mu_{\pi})^4} \int d^3h \int d^3h' \int d^3k \, \mathcal{OV}_{(L,T),SQQ3D'}$$

$$\theta(1 - |\mathbf{h}|)\theta(|\mathbf{h} - \mathbf{k}| - 1)\theta(1 - |\mathbf{h'} + \mathbf{Q}|)\theta(|\mathbf{h} - \mathbf{k} + \mathbf{Q}| - 1)$$

$$\theta(|\mathbf{h'} + \mathbf{k}| - 1)\theta(1 - |\mathbf{h'}|)$$

$$\frac{1}{k^2 - \mathbf{k} \cdot \mathbf{h} + \mathbf{k} \cdot \mathbf{h'}} \frac{1}{k^2 + \mathbf{k} \cdot (\mathbf{h'} - \mathbf{h}) + \mathbf{Q} \cdot (\mathbf{h} - \mathbf{h'} - \mathbf{k})}$$

$$\left(\frac{-1}{\pi} Im\right) \frac{1}{\nu - (k^2 + Q^2/2 + \mathbf{k} \cdot (\mathbf{h'} - \mathbf{h}) + \mathbf{Q} \cdot (\mathbf{h} - \mathbf{k})) + i\eta} . \tag{54}$$

In Eqs. (53)-(54), we have used,

$$k' = k - Q$$

and

$$\mathcal{OV}_{L,SQPD'} = \mathcal{OV}_{L,SQQ3D'} = \Gamma_{\pi}^{2}(k) \Gamma_{\pi}^{2}(k') 5\{3\tilde{g}^{\prime 2} + (\widehat{\boldsymbol{k}} \cdot \widehat{\boldsymbol{k}^{\prime}})^{2}\tilde{h}^{\prime 2} + 2\tilde{g}^{\prime}\tilde{h}^{\prime}\}, \qquad (55)$$

$$\mathcal{OV}_{T,SQPD'} = \left(\frac{\hbar c k_F}{2mc^2}\right)^2 \Gamma_{\pi}^2(k) \Gamma_{\pi}^2(k')
\left\{20[\boldsymbol{h}.(\boldsymbol{h'}+\boldsymbol{k}) - (\widehat{\boldsymbol{Q}}.\boldsymbol{h})(\widehat{\boldsymbol{Q}}.(\boldsymbol{h'}+\boldsymbol{k}))][3\tilde{g}'^2 + (\widehat{\boldsymbol{k}}.\widehat{\boldsymbol{k'}})^2 \tilde{h}'^2 + 2\tilde{g}'\tilde{h}'] + (3\mu_s^2 + 2\mu_v^2)[4Q^2\tilde{g}'^2 + (\boldsymbol{Q} \times (\boldsymbol{k} \times \boldsymbol{k'}))^2 \tilde{h}'^2 + (Q^2 + (\boldsymbol{Q}.\widehat{\boldsymbol{k'}})^2)\tilde{g}'(k)\tilde{h}'(k') + (Q^2 + (\boldsymbol{Q}.\widehat{\boldsymbol{k}})^2)\tilde{g}'(k')\tilde{h}'(k)] - (3\mu_s + 2\mu_v)\tilde{h}'^2 \frac{2}{Q^2} (\widehat{\boldsymbol{k}}.\widehat{\boldsymbol{k'}})[(\widehat{\boldsymbol{k}}.\boldsymbol{Q})(\widehat{\boldsymbol{k'}}.(\boldsymbol{h}+\boldsymbol{h'}+\boldsymbol{k})) - (\widehat{\boldsymbol{k'}}.\boldsymbol{Q})(\widehat{\boldsymbol{k}}.(\boldsymbol{h}+\boldsymbol{h'}+\boldsymbol{k'}))]\right\}, \tag{56}$$

and

$$\mathcal{OV}_{T,SQQ3D'} = \left(\frac{\hbar c k_F}{2mc^2}\right)^2 \Gamma_{\pi}^2(k) \Gamma_{\pi}^2(k')
\left\{20[\boldsymbol{h'}.(\boldsymbol{h}-\boldsymbol{k}) - (\widehat{\boldsymbol{Q}}.\boldsymbol{h'})(\widehat{\boldsymbol{Q}}.(\boldsymbol{h}-\boldsymbol{k}))][3\tilde{g}'^2 + (\widehat{\boldsymbol{k}}.\widehat{\boldsymbol{k'}})^2 \tilde{h}'^2 + 2\tilde{g}'\tilde{h}'] + (3\mu_s^2 + 2\mu_v^2)[4Q^2\tilde{g}'^2 + (\boldsymbol{Q}\times(\boldsymbol{k}\times\boldsymbol{k'}))^2\tilde{h}'^2 + (Q^2 + (Q.\widehat{\boldsymbol{k}})^2)\tilde{g}'(k)\tilde{h}'(k') + (Q^2 + (Q.\widehat{\boldsymbol{k}})^2)\tilde{g}'(k')\tilde{h}'(k)] - (3\mu_s + 2\mu_v)\tilde{h}'^2 \frac{2}{Q^2} (\widehat{\boldsymbol{k}}.\widehat{\boldsymbol{k'}})[(\widehat{\boldsymbol{k}}.\boldsymbol{Q})(\widehat{\boldsymbol{k'}}.(\boldsymbol{h}+\boldsymbol{h'}-\boldsymbol{k})) - (\widehat{\boldsymbol{k'}}.\boldsymbol{Q})(\widehat{\boldsymbol{k}}.(\boldsymbol{h}+\boldsymbol{h'}-\boldsymbol{k'}))]\right\}.$$
(57)

Graph SQQ1E of Fig. 3:

$$(S_{SQQ1E}(\boldsymbol{Q}, \nu))_{L,T} = -\frac{A}{(2\pi)^5} \left(\frac{f_{\pi}^2}{4\pi\hbar c}\right)^2 \frac{9(mc^2)^3}{4(\hbar c\mu_{\pi})^4} \int d^3p \int d^3k \int d^3k'$$

$$\mathcal{O}\mathcal{V}_{(L,T),SQQ1E}\theta(|\boldsymbol{p}|-1)\theta(1-|\boldsymbol{p}+\boldsymbol{k}|)\theta(|\boldsymbol{p}+\boldsymbol{Q}|-1)$$

$$\theta(1-|\boldsymbol{h}+\boldsymbol{k'}|)\theta(|\boldsymbol{p}+\boldsymbol{k}+\boldsymbol{k'}|-1)$$

$$\frac{1}{(\boldsymbol{k}.\boldsymbol{k'})^2} \left(\frac{-1}{\pi} Im\right) \left[\frac{1}{\nu-(Q^2/2+\boldsymbol{Q}.\boldsymbol{p}+\boldsymbol{k'}.\boldsymbol{k})+i\eta}\right]. \tag{58}$$

Finally, graph SQQ2E of Fig. 3:

$$(S_{SQQ2E}(\boldsymbol{Q}, \nu))_{L,T} = -\frac{A}{(2\pi)^5} \left(\frac{f_{\pi}^2}{4\pi\hbar c}\right)^2 \frac{9(mc^2)^3}{4(\hbar c\mu_{\pi})^4} \int d^3h \int d^3k \int d^3k'$$

$$\mathcal{OV}_{(L,T),SQQ2E}\theta(1 - |\boldsymbol{h}|)\theta(|\boldsymbol{h} - \boldsymbol{k}| - 1)\theta(|\boldsymbol{h} - \boldsymbol{k'}| - 1)$$

$$\theta(1 - |\boldsymbol{h} - \boldsymbol{Q}|)\theta(1 - |\boldsymbol{h} - \boldsymbol{k} - \boldsymbol{k'}|)$$

$$\frac{1}{(\boldsymbol{k}.\boldsymbol{k'})^2} \left(\frac{-1}{\pi} Im\right) \left[\frac{1}{\nu - (Q^2/2 + \boldsymbol{Q}.\boldsymbol{h} - \boldsymbol{k'}.\boldsymbol{k}) + in}\right], \tag{59}$$

where

$$\mathcal{OV}_{L,SQQ1E} = \mathcal{OV}_{L,SQQ2E} = \mathcal{OV}_{L,SE2E} , \qquad (60)$$

$$\mathcal{OV}_{T,SQQ1E} = (\frac{\hbar c k_F}{2mc^2})^2 \Gamma_{\pi}^2(k) \Gamma_{\pi}^2(k') \{ [\boldsymbol{p}^2 - (\widehat{\boldsymbol{Q}} \cdot \boldsymbol{p})^2] + Q^2(\mu_s^2 + \mu_v^2))/4 \}$$

$$[3\tilde{g}'^2 - (2(\widehat{\boldsymbol{k}} \cdot \widehat{\boldsymbol{k'}})^2 - 1)\tilde{h}'^2 + 2\tilde{g}'\tilde{h}'], \qquad (61)$$

 $\quad \text{and} \quad$

$$\mathcal{OV}_{T,SQQ2E} = (\frac{\hbar c k_F}{2mc^2})^2 \Gamma_{\pi}^2(k) \Gamma_{\pi}^2(k') \{ [\boldsymbol{h}^2 - (\widehat{\boldsymbol{Q}} \cdot \boldsymbol{h})^2] + Q^2 (\mu_s^2 + \mu_v^2))/4 \}$$

$$[3\tilde{g}'^2 - (2(\widehat{\boldsymbol{k}} \cdot \widehat{\boldsymbol{k'}})^2 - 1)\tilde{h}'^2 + 2\tilde{g}'\tilde{h}'] . \tag{62}$$

REFERENCES

- [1] S. Boffi, C. Giusti, F. Pacati and M. Radici in *Electromagnetic Response of Atomic Nuclei*, Clarendon Press, Oxford 1996.
- [2] P. Barreau *et al.*, Nucl. Phys. **A402**, 515 (1983).
- [3] Z. E. Meziani *et al.*, Phys. Rev. Lett. **52**, 2130 (1984).
- [4] Z. E. Meziani et al., Phys. Rev. Lett. 55, 1233 (1985).
- [5] C. C. Blatchley, J. J. LeRose, O. E. Pruet, D. Zimmermann, C. F. Williamsom and M. Deady, Phys. Rev. C34, 1243 (1986).
- [6] C. F. Williamson, private communication.
- [7] J. Jourdan, Nucl. Phys. **A603**, 117 (1996).
- [8] J. V. Noble, Phys. Rev. Lett. 46, 412 (1981); Phys. Rev. C27, 423 (1983).
- [9] G. Do Dang and Nguyen van Giai, Phys. Rev. C30, 731 (1984).
- [10] H. Kurasawa and T. Suzuki, Nucl. Phys. **A454**, 527 (1986).
- [11] E. N. Nikolov, M. Bergmann, Chr. V. Christov, K. Goeke, A. N. Antonov and S. Krewald, Phys. Lett. B281, 208 (1992).
- [12] M. Cavinato, D. Drechsel, E. Fein, M. Marangoni and A. M. Saruis, Nucl. Phys. A423, 376 (1984).
- [13] S. Drożdż, G. Co', J. Wambach and J. Speth, Phys. Lett. **B185**, 287 (1987).
- [14] G. Co', K. F. Quader, R. D. Smith, J. Wambach, Nucl. Phys. A485, 61 (1988).
- [15] S. Drożdż, S. Nishizaki, J. Speth and J. Wambach, Phys. Rep. 197, 1 (1990).
- [16] A. Fabrocini and S. Fantoni, Nucl. Phys. A503, 375 (1989); A. Fabrocini, Phys. Rev. C55, 338 (1997).
- [17] Y. Horikawa, F. Lenz and Nimai C. Mukhopadhyay, Phys. Rev. C22, 1680 (1980).
- [18] C. R. Chinn, A. Picklesimer and J. W. Van Orden, Phys. Rev. C40, 790 (1989).
- [19] A. Picklesimer, J. W. Van Orden and S. J. Wallace, Phys. Rev. C32, 1312 (1985);
 C. R. Chinn, A. Picklesimer and J. W. Van Orden, Phys. Rev. C40, 1159 (1989).
- [20] F. Capuzzi, C. Giusti and F. D. Pacati, Nucl. Phys. **A524**, 681 (1991).
- [21] F. Capuzzi, Nucl. Phys. **A554**, 362 (1993).
- [22] P. M. Boucher, B. Castel and Y. Okuhara, Ann. Phys. (N.Y.) 196, 150 (1989).
- [23] W. M. Alberico, M. Ericson and A. Molinari, Ann. Phys. (N.Y.) **154**, 356 (1984).
- [24] W. M. Alberico, A. De Pace, A. Drago and A. Molinari, Rivista del Nuovo Cimento 14, 1 (1991).
- [25] K. Takayanagi, K. Shimizu and A. Arima, Nucl. Phys. A477, 205 (1988).
- [26] K. Takayanagi, Nucl. Phys. **A522**, 523 (1991).
- [27] K. Takayanagi, Phys. Lett. B230, 11 (1989); Nucl. Phys. A510, 162 (1990); Nucl. Phys. A522, 494 (1991); Nucl. Phys. A556, 14 (1993).
- [28] E. Bauer, Phys. Rev. C43, 2438 (1991).
- [29] A. De Pace and M. Viviani, Phys. Rev. C48, 2931 (1993).
- [30] E. Bauer, Nucl. Phys. **A589**, 669 (1995).
- [31] E. Bauer, A. Ramos and A. Polls, Phys. Rev. C54, 2959 (1996).
- [32] A. Polls, A. Ramos and W.H. Dickohff, in "Two nucleon emission reactions", eds. O. Benhar and A. Fabrocini (ETS, Pisa, 1990) 374.
- [33] C.C. Gearhart, W.H. Dickhoff, A. Polls and A. Ramos, Int. Jour. Mod. Phys. 5, 461 (1996).
- [34] A. Gil, J. Nieves and E. Oset, Nucl. Phys. **A627**, 543 (1997).

- [35] J. E. Amaro, A. M. Lallena, Nucl. Phys. A537, 585 (1992); J. E. Amaro, G. Co', A. M. Lallena, Ann. Phys. (N.Y.) 221, 306 (1993).
- [36] Y. Jin, D. S. Onley and L. E. Wright, Phys. Rev. C45, 1333 (1992).
- [37] T. Shigehara, K. Shimizu and A. Arima, Nucl. Phys. **A492**, 388 (1989).
- [38] M. Buballa, S. Drożdź, S. Krewald and J. Speth, Ann. Phys. (N.Y.) 208, 346 (1991).

TABLES

TABLE I. Free and Self-energy contributions to the Longitudinal and Transverse structure function (multiplied by 10^5). All results are for nuclear matter at momentum transfer q = 410 MeV/c in units of MeV^{-1} fm⁻³. The first column represents the energy transfer in MeV. Column Lind. represents the free structure function. Columns SE13 give the direct (D) and exchange (E) contribution to the diagonal part of the self-energy up to infinite order. Their first contributions are the graphs $SE1_D$, $SE3_D$, $SE1_E$, and $SE3_E$ of Fig. 1. Columns $SE2_D$, $SE2_E$ and $SE2_{E'}$ are the non-diagonal self-energy contributions to the structure function as shown in Fig. 1. The last column is the sum of all these contributions given by Eq. (21).

long.							
$\hbar\omega$	Lind.	$SE13_D$	$SE13_E$	$SE2_D$	$SE2_{E}$	$SE2_{E'}$	$S^{Lind.+SE.}$
50.	38.729	-1.269	0.715	-1.570	0.185	0.071	36.862
100.	46.106	-4.390	0.599	-0.559	0.374	0.159	42.289
150.	41.357	-5.949	0.397	1.085	-0.096	-0.050	36.743
200.	24.481	-3.250	0.111	2.219	-0.045	-0.027	23.490
250.	0.000	2.971	-0.127	0.521	-0.004	-0.005	3.357
\overline{trans} .							
50.	60.380	-1.938	1.112	-3.205	0.037	0.181	56.566
100.	72.299	-6.943	0.946	-0.604	0.119	0.004	65.821
150.	64.610	-9.354	0.621	2.575	-0.071	-0.232	58.149
200.	37.739	-4.948	0.164	5.337	-0.082	-0.357	37.853
250.	0.000	4.587	-0.195	0.726	-0.006	-0.079	5.032

TABLE II. RPA-type contributions to the Transverse structure function (multiplied by 10^5) in units of MeV⁻¹ fm⁻³ for nuclear matter at momentum transfer q=410 MeV/c. Columns $RPA1_D$ ($RPA1_E$) and $RPA2_D$ ($RPA2_{(E+E')}$) are the first and second order direct (exchange)-part to the RPA response, respectively. The notation is the same as in Fig. 1. Note that in that figure only forward-going contributions are shown while the present results contain both forward and backward-going contributions. Column $RPA12_{D+E}$ is the sum of all first and second order contributions (given by Eqs. (22) and (23)). Finally, column RPA_{ant} is the result for a full antisymmetric RPA using the formalism given in Ref. [31].

$\hbar\omega$					$RPA12_{D+E}$	$RPA_{ant.}$
	$RPA1_D$	$RPA1_E$	$RPA2_D$	$RPA2_{(E+E')}$		
50.	-30.233	8.844	9.028	-2.912	-15.273	-19.527
100.	-13.801	4.209	-3.098	0.914	-11.775	-9.988
150.	5.122	-1.132	-3.441	1.204	1.753	3.307
200.	10.354	-3.206	1.468	-0.466	8.150	7.186
250.	0.000	0.000	0.000	0.000	0.000	0.000

TABLE III. Longitudinal and Transverse S_{QP} -type structure function (multiplied by 10^5) in units of MeV⁻¹ fm⁻³ for nuclear matter at momentum transfer q=410 MeV/c. The notation SQP_D to $SQP_{D'}$ is the same as in Fig. 2. Column SQP_{ant} is the sum of all contributions.

long.					
$\hbar\omega$	SQP_D	SQP_E	$SQP_{E'}$	$SQP_{D'}$	SQP_{ant}
50.	4.950	-0.003	-0.077	1.101	5.971
100.	4.136	-0.016	-0.110	1.142	5.152
150.	3.116	-0.055	-0.075	0.589	3.575
200.	1.598	-0.037	-0.007	0.234	1.789
250.	-1.284	0.004	0.022	-0.058	-1.316
\overline{trans} .					
50.	7.469	-0.604	-0.101	1.324	8.089
100.	5.412	-0.672	-0.144	1.374	5.969
150.	3.656	-0.436	-0.098	0.928	4.049
200.	0.906	-0.001	-0.009	0.491	1.387
250.	-3.652	0.341	0.029	-0.073	-3.356

TABLE IV. Longitudinal and Transverse S_{QQ} -type structure function. The notation $SQQ1_D$ to $SQQ3_D$ is the same as in Fig. 3. $SQQ3_{Etot.}$ is the sum of $SQQ3_E$, $SQQ3_{E'}$ and $SQQ3_{D'}$ from the same figure. Column SQQ_{ant} is the sum of all contributions.

long.							
$\hbar\omega$	$SQQ1_D$	$SQQ1_E$	$SQQ2_D$	$SQQ2_E$	$SQQ3_D$	$SQQ3_{Etot.}$	SQQ_{ant}
50.	4.692	-0.042	2.455	-0.074	-0.552	0.041	6.520
100.	8.535	-0.327	1.428	-0.046	-0.629	0.042	9.003
150.	9.807	-0.344	0.661	-0.019	-0.299	0.029	9.834
200.	10.426	-0.278	0.310	-0.008	-0.220	0.020	10.249
250.	10.342	-0.167	0.047	-0.003	-0.113	0.011	10.118
\overline{trans} .							
50.	6.064	-0.051	4.413	-0.062	-1.614	0.012	8.762
100.	12.673	-0.307	2.493	-0.027	-2.230	0.017	12.617
150.	15.153	-0.313	1.179	-0.007	-1.848	0.014	14.178
200.	17.352	-0.263	0.559	-0.003	-0.467	0.012	17.188
250.	16.551	-0.167	0.090	-0.001	-0.271	0.006	16.208

TABLE V. Comparison between our results and the corresponding direct values calculated with a modified value of the g'-Landau Migdal parameter (g' = 0.5) to partially reproduce the exchange contributions. Our results are given by SPP_{ant} , SQP_{ant} and SQQ_{ant} where a value g' = 0.7 was employed with the explicit inclusion of exchange graphs.

long.						
$\hbar\omega$	SPP_{ant}	$SPP_{dir,g'=.5}$	SQP_{ant}	$SQP_{dir,g'=.5}$	SQQ_{ant}	$SQQ_{dir,g'=.5}$
50.	36.862	36.409	5.971	5.034	6.520	2.529
100.	42.289	43.256	5.152	5.442	9.003	4.995
150.	36.743	36.430	3.575	4.312	9.834	5.971
200.	23.490	19.059	1.789	0.966	10.249	6.291
250.	3.357	2.393	-1.316	-1.336	10.118	6.015
\overline{trans} .						
$\hbar\omega$	SPP_{ant}	$SPP_{dir,g'=.5}$	SQP_{ant}	$SQP_{dir,g'=.5}$	SQQ_{ant}	$SQQ_{dir,g'=.5}$
50.	37.039	47.428	7.109	5.533	8.762	5.049
100.	55.833	63.337	5.362	5.719	12.617	9.092
150.	61.456	59.066	4.049	3.864	14.178	10.814
200.	45.039	33.882	1.727	1.392	17.188	11.586
250.	5.032	3.719	-3.356	-1.883	16.208	10.800

FIGURES

- FIG. 1. Goldstone diagrams stemming from Eqs. (21)-(23). In every diagram the wavy lines represent the external probe with energy momentum (\mathbf{q}, ω). The dashed line is the residual interaction. For simplicity we show only forward-going contributions, where the incoming external probe creates a particle-hole pair. In the backward-going diagrams (not represented here) the probe can also destroy a particle-hole pair.
- FIG. 2. The same as Fig. 1 but for the S_{QP} -channel given by Eq. (26). The action of the external probe represents the interference between scattering (a particle or a hole) and creating (or destroying) a particle-hole pair.
- FIG. 3. The same as Fig. 1 but for the S_{QQ} -channel given by Eq. (27). The action of the external probe is to create (or destroy) a particle-hole pair.

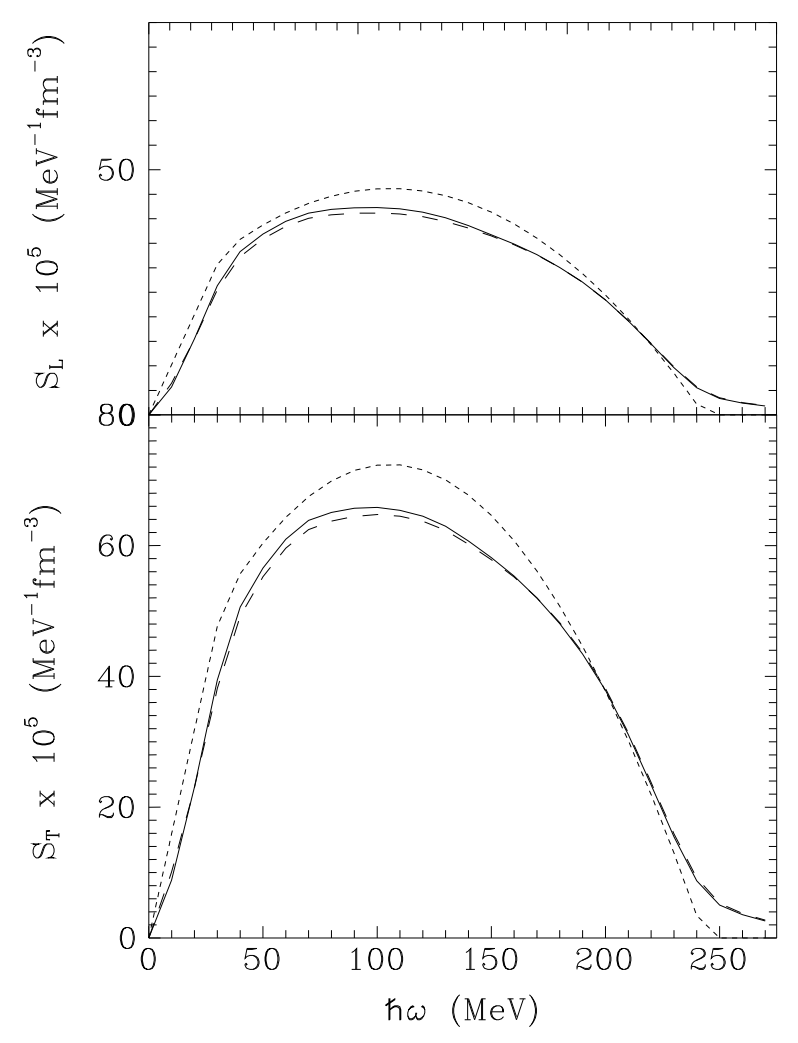


FIG. 4. Self-energy contributions to the longitudinal (upper part) and transverse (lower part) structure function of nuclear matter at momentum transfer $q=410~{\rm MeV/c}$. Short-dashed line: Lindhard function using an effective mass $m^*/m=0.85$. Long-dashed line: effect of adding the direct self-energy terms. Full line: effect of adding the direct and exchange self-energy terms.

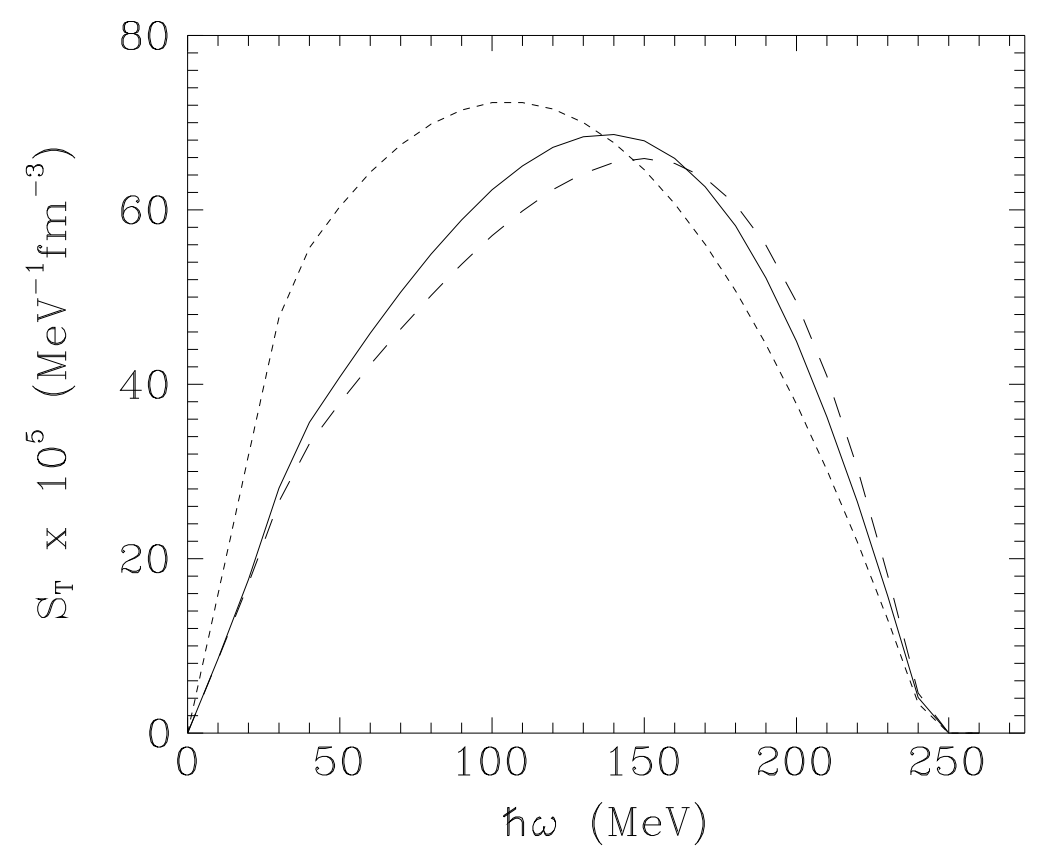


FIG. 5. RPA contributions to the transverse structure function of nuclear matter at q=410 MeV/c. Short-dashed line: Lindhard function ($m^*/m=0.85$). Long-dashed line: direct ring diagrams. Full line: full RPA structure function including the exchange terms to all orders.

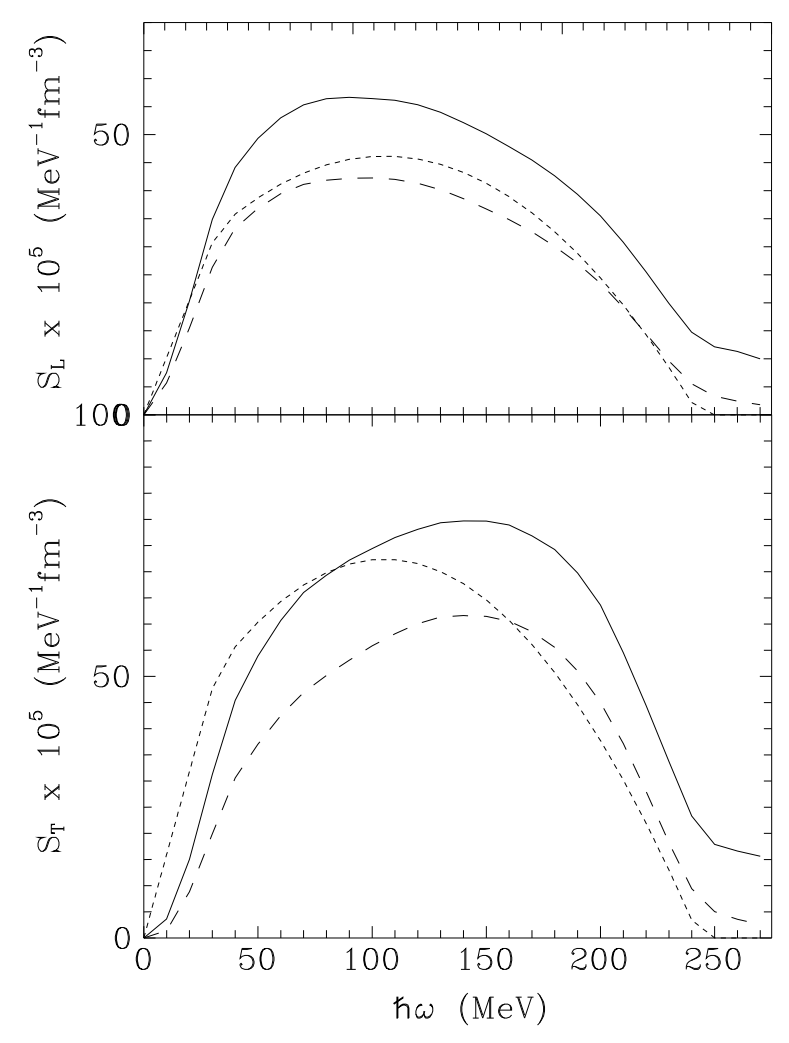


FIG. 6. Contribution of ground state correlations to the longitudinal (upper part) and transverse (lower part) structure function of nuclear matter at momentum transfer q=410 MeV/c. Short-dashed line: Lindhard function ($m^*/m=0.85$). Long-dashed line: S_{PP} structure function. Full line: inclusion of the ground state correlation diagrams to the S_{PP} structure function.